

H-TMD with hybrid control method for vibration control of long span cable-stayed bridge

Bing Han^{*1,2}, Wu Tong Yan^{1a}, Viet Hung Cu^{1b}, Li Zhu^{1c} and Hui Bing Xie^{1d}

¹School of Civil Engineering, Beijing Jiaotong University, No.3, Shangyuancun, Haidian district, Beijing 100044, China

²Key Laboratory of Safety and Risk Management on Transport Infrastructures, Ministry of Transport, PRC, Beijing 100044, China

(Received October 10, 2017, Revised February 5, 2019, Accepted February 9, 2019)

Abstract. Long span cable-stayed bridges are extremely vulnerable to dynamic excitations such as which caused by traffic load, wind and earthquake. Studies on cable-stayed bridge vibration control have been keenly interested by researchers and engineers in design new bridges and assessing in-service bridges. In this paper, a novel Hybrid-Tuned Mass Damper (H-TMD) is proposed and a hybrid control model named Mixed Logic Dynamic (MLD) is employed to build the bridge-H-TMD system to mitigate the vibrations. Firstly, the fundamental theory and modeling process of MLD model is introduced. After that, a new state switching design of the H-TMD and state space equations for different states are proposed to control the bridge vibrations. As the state switching designation presented, the H-TMDs can applied active force to bridge only if the structural responses are beyond the limited thresholds, otherwise, the vibrations can be reduced by passive components of dampers without active control forces provided. A new MLD model including both passive and active control states is built based on the MLD model theory and the state switching design of H-TMD. Then, the case study is presented to demonstrate the proposed methodology. In the case study, the control scheme with H-TMDs is applied for a long span cable-stayed bridge, and the MLD model is established and simulated with earthquake excitation. The simulation results reveal that the suggested method has a well damping effect and the established system can be switched between different control states as design excellently. Finally, the energy consumptions of H-TMD schemes are compared with that of Active Tuned Mass Damper (ATMD) schemes under variable seismic wave excitations. The compared results show that the proposed H-TMD can save energy than ATMD.

Keywords: cable-stayed bridge; hybrid control; H-TMD; MLD; ATMD; state switching

1. Introduction

With lately blooming advances in materials and construction technologies, the selection of cable-stayed bridge is a probably option of owners. Not only giving a huge navigational clearance for container ships, a cable-stayed bridge also provides a great view that makes the bridge to be the landmark of its vicinity. Since the cable-stayed bridge becomes longer, lighter and more flexible, and its natural frequencies are closely spaced, leading to become vulnerable to violent vibration induced by traffic load, wind and earthquake. In general, mitigation of undesired bridge vibrations can be achieved by attaching damping devices in structures based on theories of passive, semi-active and active control methods.

Nowadays, passive dampers such as viscous damper (VD) and tuned mass damper (TMD) etc. have been widely used to reduce the structural vibrations. Huang (2018) studied the damping effects of VD in steel frames under strong earthquakes with the optimized distributions of dampers. Yu *et al.* (2018) utilized VDs to reduce the longitudinal structural responses of a large freight railway cable-stayed bridge under braking forces. Meanwhile, TMD was also widely analyzed and employed by researchers to reduce wind, crowd and ground motion induced vibrations of the structures (Nimmen *et al.* 2016, Quaranta *et al.* 2016, Xing *et al.* 2014). Besides, some novel passive devices were also proposed and studied to mitigate structural vibrations, such as tuned particle damper (Yan *et al.* 2014) and tuned viscous mass damper (Ikago *et al.* 2012). However, the previous experiences point out that the passive control devices have some shortcomings such as they are sensitivity to the excitation frequency, worse robustness and limited effects.

To overcome the drawbacks of the passive control system, active control systems have been studied and developed. Nigdeli *et al.* (2013) studied active tendons to control vibrations of multistory structures and designed the PID controller to obtain the optimal control force. The Active Tuned Mass Damper (ATMD) has been also applied for structure vibration reduction in the engineering practice (Venzani *et al.* 2013, He and Li 2014). Nevertheless, the huge energy consumption and vulnerability of the active

*Corresponding author, Professor

E-mail: bhan@bjtu.edu.cn

^aPh.D. Student

E-mail: yanwutong@bjtu.edu.cn

^bPh.D. Student

E-mail: 13119006@bjtu.edu.cn

^cAssociate Professor

E-mail: zhuli@bjtu.edu.cn

^dLecture

E-mail: hbxie@bjtu.edu.cn

control device decrease its reliability.

Due to their characteristics of energy conservation and effectiveness, semi-active controls have been popularly employed. Semi-active controls depend on the various characteristics of the intelligent material property, and they change their stiffness and damping by changing the voltage of the device to reduce the structural vibration responses (Xu *et al.* 2006). So far, variable types of control equipment (Ghorbani-Tanha *et al.* 2011, Lin *et al.* 2013) and control algorithm (Askari *et al.* 2016, Pourzeynali *et al.* 2016) have been proposed to improve and develop the semi-active control schemes, which have more developmental foreground.

In this paper, a novel hybrid control method with switching of active and passive states is proposed and designed based on consideration of the effectiveness and energy conservation to control the vibrations of the cable-stayed bridge. In the proposed method, H-TMD is employed as the control device and Mixed Logic Dynamic (MLD) model is used as the control model to realize the integration of different control states. When the vibration amplitude of the structure is low, the vibration is reduced by passive parts of the H-TMD as tuning and damping effects. Otherwise, the control actuator is triggered to provide control force to the structure once the violent oscillatory motion is happened. In addition, the 3rd Nanjing Yangtze River Bridge in China is chosen as a case study to justify the effectiveness of the proposed method. The influences of various parameters on theoretically dynamical response of the bridge, such as damping effect, state-switching and energy consumption are analyzed and discussed in detail.

2. Fundamental theory of MLD model

Hybrid system (HS) is denoted as dynamical processes including three components, including continuous dynamic, discrete dynamic and the interaction between them, as shown in Fig. 1. Discrete components of the system are driven by emergencies, such as on/off switches or valves, gears or speed selectors, and continuous components are evolved with the development of states. Discrete events change the evolutionary direction of the continuous state and continuous components decide the driving status of discrete events. The interactions between discrete events and continuous components make the system discrete overall and continuous locally.

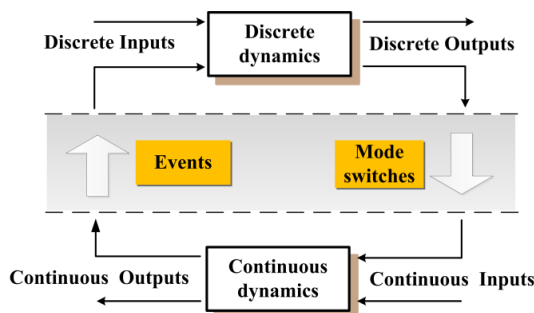


Fig. 1 Components of hybrid system

Hybrid system can be described in multiple models, for example, Piece Wise Affine (PWA) systems (Guezar *et al.* 2011), Linear Complementarity (LC) systems (Vieira *et al.* 2017), Extended Linear Complementarity (ELC) systems (Yu *et al.* 2009) and Mixed Logic Dynamic (MLD) systems (Sirmatel and Geroliminis 2018, Bemporad and Morari 1999). One of them, MLD model has a straightforward description and rigorous logic rules, and it can be transformed into different models. Therefore, it is preferred as the H-TMD-hybrid control model in this paper.

2.1 Introduction of MLD

MLD was first proposed by Bemporad and Morari (1999) as a new modeling method for process control, and now are applied to public transport operations (Sirmatel and Geroliminis 2018), air suspension system (Sun *et al.* 2017), intelligent vehicle (Sun *et al.* 2019) and so on. It was described by interdependent logic rules, operation constraints and physical laws, and considered the logical judgments and constrains-heuristic knowledge as the propositional logic. According to the relationship between logical operators and propositions, logical variables were transformed into the integer linear inequalities. The combination of the logical variables and state space equations denoted the interaction of continuous dynamic and logical events.

The general equation of MLD can be expressed as

$$\begin{cases} \mathbf{x}(t+1) = \mathbf{A}\mathbf{x}(t) + \mathbf{B}_1\mathbf{u}(t) + \mathbf{B}_2\boldsymbol{\delta}(t) + \mathbf{B}_3\mathbf{z}(t) \\ \mathbf{y}(t) = \mathbf{C}\mathbf{x}(t) + \mathbf{D}_1\mathbf{u}(t) + \mathbf{D}_2\boldsymbol{\delta}(t) + \mathbf{D}_3\mathbf{z}(t) \\ \mathbf{E}_2\boldsymbol{\delta}(t) + \mathbf{E}_3\mathbf{z}(t) \leq \mathbf{E}_1\mathbf{u}(t) + \mathbf{E}_4\mathbf{x}(t) + \mathbf{E}_5 \end{cases} \quad (1)$$

where $\mathbf{x}(t)$, $\mathbf{u}(t)$ and $\mathbf{y}(t)$ are the states, inputs and outputs of the system respectively (they can be either discrete variables or continuous variables or both of two types); $\mathbf{z}(t)$ and $\boldsymbol{\delta}(t)$ are introduced auxiliary continuous variables and auxiliary logical variables respectively; and \mathbf{A} , \mathbf{B}_i , \mathbf{C} , \mathbf{D}_i , \mathbf{E}_i are parameter matrixes of the system.

2.2 Modeling process

The modeling process of the MLD can be divided into four steps (Sirmatel and Geroliminis 2018),

(1) According to the dynamic theory, the state space equations of continuous dynamic state of the system can be established firstly.

(2) Building the propositional logic based on the system qualitative knowledge and logic constraints. Logical variables $\delta_p \in \{1,0\}$ denote true or false of proposition P_i , and it transforms simple propositions P_1, P_2, \dots, P_r into compound propositions by logical operator $\vee, \wedge, \oplus, \rightarrow, \neg, \leftrightarrow$, etc., then the compound propositions can be described by the integer linear inequality of logical variables $\delta_1, \delta_2, \dots, \delta_p$. The basic transformation relationship can be denoted as

$$\begin{aligned} P_1 \vee P_2 \vee \dots \vee P_r &\leftrightarrow \delta_1 + \delta_2 + \dots + \delta_p \geq 1 \\ P_1 \wedge P_2 \wedge \dots \wedge P_r &\leftrightarrow \delta_1 \geq 1; \delta_2 \geq 1; \dots; \delta_p \geq 1 \\ P_1 \oplus P_2 \oplus \dots \oplus P_r &\leftrightarrow \delta_1 + \delta_2 + \dots + \delta_p = 1 \end{aligned} \quad (2)$$

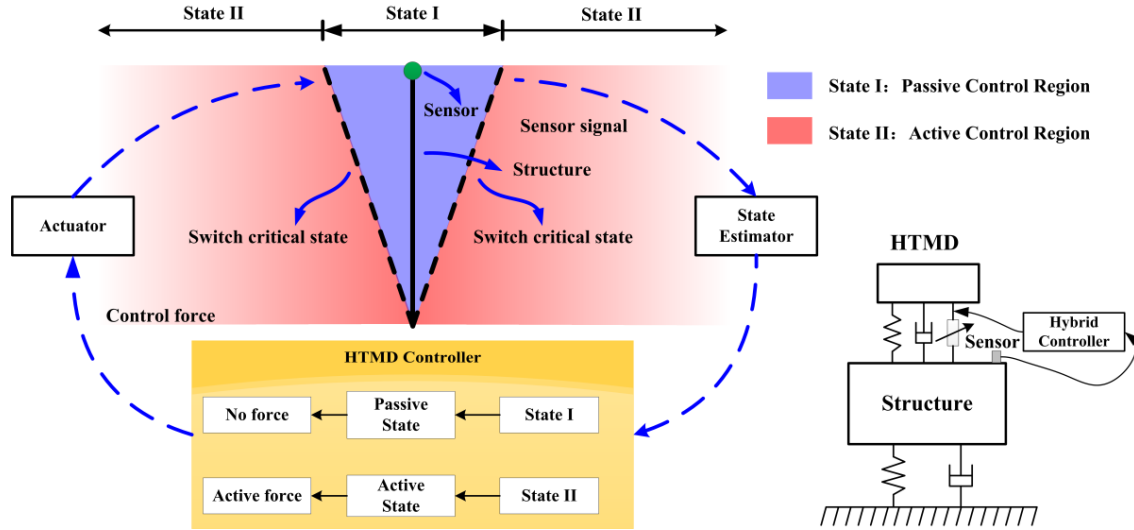


Fig. 2 Design of H-TMD and state switching

Relate to the inequality constraint conditions $\mathbf{a}^T \mathbf{x} \leq 0$, the propositional form can be established as

$$[f(\mathbf{x}) = \mathbf{a}^T \mathbf{x} \leq 0] \leftrightarrow [\delta = 1] \quad (3)$$

The mixed integer linear inequalities can be yielded from Eq. (3) as shown in Eq. (4)

$$\begin{cases} f(\mathbf{x}) \leq \mathbf{M}(1-\delta) \\ f(\mathbf{x}) \geq \boldsymbol{\varepsilon} + (\mathbf{m} - \boldsymbol{\varepsilon})\delta \end{cases} \quad (4)$$

where $\mathbf{x} \in \mathbf{X} \in \mathbf{R}^n$ is continuous variable; $\mathbf{M} = \max f(\mathbf{x})$ and $\mathbf{m} = \min f(\mathbf{x})$ are the upper-lower limit lines of $f(\mathbf{x})$ respectively.

(3) Auxiliary variable $\mathbf{Z} = \delta f(\mathbf{x})$ is introduced to denote the coupling relationship between continuous and discrete variables, then the mixed integer linear inequalities are presented correspondingly, as shown in Eq. (5).

$$\begin{aligned} \delta = \delta_1 \delta_2 \Leftrightarrow & \begin{cases} -\delta_1 + \delta \leq 0 \\ -\delta_2 + \delta \leq 0 \\ \delta_1 + \delta_2 - \delta \leq 1 \end{cases} \\ \Gamma = \delta f(\mathbf{x}) \Leftrightarrow & \begin{cases} \Gamma \leq \mathbf{M}\delta \\ \Gamma \geq \mathbf{m}\delta \\ \Gamma \leq f(\mathbf{x}) - \mathbf{m}(1-\delta) \\ \Gamma \geq f(\mathbf{x}) - \mathbf{M}(1-\delta) \end{cases} \end{aligned} \quad (5)$$

(4) Introducing auxiliary variables and logic into the linear equations of discrete system and describing the continuous and logic parts of the system in a unified framework, which can guarantee the stability of the system and reduce the oscillation of the system when switching between different states.

Based on four steps mentioned above, the whole hybrid system can be denoted as Eq. (1), where the first equation $\mathbf{x}(t+1) = \mathbf{A}\mathbf{x}(t) + \mathbf{B}_1\mathbf{u}(t) + \mathbf{B}_2\boldsymbol{\delta}(t) + \mathbf{B}_3\mathbf{z}(t)$ is the evolution equation, the second equation $\mathbf{y}(t) = \mathbf{C}\mathbf{x}(t) + \mathbf{D}_1\mathbf{u}(t) + \mathbf{D}_2\boldsymbol{\delta}(t) + \mathbf{D}_3\mathbf{z}(t)$ is the output equation and the inequalities $\mathbf{E}_2\boldsymbol{\delta}(t) + \mathbf{E}_3\mathbf{z}(t) \leq \mathbf{E}_1\mathbf{u}(t) + \mathbf{E}_2\mathbf{x}(t) + \mathbf{E}_5$ is the constraints and the state switching conditions of the system.

3. Modeling method of bridge and H-TMD hybrid control system

3.1 State switching design of H-TMD

H-TMD is a special TMD which is designed by adding an actuator into passive TMD so that it can apply control force to structure selectively with the feedback response of the structure, as shown in Fig. 2. When the vibration occurs, the sensors transfer signal to the state estimator then the structural state and the response at monitoring location is estimated. According to the estimated response, H-TMD controller calculates and decides the control states and control forces needed to apply to the structure. It means that the H-TMD plays a role of passive TMD which does not apply control force to the structure if the corresponding monitoring response is within the control thresholds (State I). On the contrary, H-TMD provides feedback control force according to certain control algorithm to reduce the vibration of the structure (State II).

3.2 State space equations of bridge-H-TMDs system

The motion equation of n-DOFs structure with m numbers of H-TMDs is expressed as follows

$$\begin{aligned} \mathbf{M}_s \ddot{\mathbf{q}} + \mathbf{C}_s \dot{\mathbf{q}} + \mathbf{K}_s \mathbf{q} &= -\mathbf{M}_s \boldsymbol{\delta} \ddot{\mathbf{x}}_g + \mathbf{P}_g^T \mathbf{f}_d \\ \mathbf{m}_d \ddot{\mathbf{q}}_d + \mathbf{f}_d &= -\mathbf{m}_d \boldsymbol{\delta}_d \ddot{\mathbf{x}}_g \\ f_{di} &= c_{di}(\dot{q}_{di} - \dot{q}_i) + k_{di}(q_{di} - q_i) - u_{di} \end{aligned} \quad (6)$$

where \mathbf{M}_s , \mathbf{C}_s and \mathbf{K}_s are the mass, stiffness and damping matrix of the structure; $\boldsymbol{\delta}$ is the direction vector of the ground acceleration; \mathbf{P}_g^T is the transformation matrix of the dampers' installation locations; $\mathbf{f}_d = [f_{d1} \ f_{d2} \ \dots \ f_{dm}]^T$ is the vector of the damping force; and c_{di} , k_{di} and u_{di} are the damping, stiffness and control force of the i^{th} damper respectively.

According to generalized coordinate transformation $\mathbf{q} = \boldsymbol{\Phi}\mathbf{Y}$, Eq. (6) can be expressed as Eq. (7), in which

$$\widehat{\mathbf{M}}_s = \Phi^T \mathbf{M}_s \Phi, \quad \widehat{\mathbf{C}}_s = \Phi^T \mathbf{C}_s \Phi \quad \text{and} \quad \widehat{\mathbf{K}}_s = \Phi^T \mathbf{K}_s \Phi.$$

$$\begin{aligned} \widehat{\mathbf{M}}_s \ddot{\mathbf{Y}} + \widehat{\mathbf{C}}_s \dot{\mathbf{Y}} + \widehat{\mathbf{K}}_s \mathbf{Y} &= -\Phi^T \mathbf{M}_s \delta \ddot{\mathbf{x}}_g + \Phi^T \mathbf{P}_g^T \mathbf{f}_d \\ \mathbf{m}_d \ddot{\mathbf{q}}_d + \mathbf{f}_d &= -\mathbf{m}_d \ddot{\mathbf{x}}_g \\ \mathbf{f}_d &= \mathbf{c}_d (\dot{\mathbf{q}}_d - \mathbf{P}_g \Phi \dot{\mathbf{Y}}) + \mathbf{k}_d (\mathbf{q}_d - \mathbf{P}_g \Phi \mathbf{Y}) - \delta_d \mathbf{u}_d \end{aligned} \quad (7)$$

Supposing $\mathbf{Z}=[\mathbf{Y}; \mathbf{q}_d]$, Eq. (7) can be rewritten as

$$\begin{aligned} \mathbf{M} \ddot{\mathbf{Z}} + \mathbf{C} \dot{\mathbf{Z}} + \mathbf{K} \mathbf{Z} + \mathbf{H} \mathbf{c}_d \mathbf{H}^T \dot{\mathbf{Z}} + \mathbf{H} \mathbf{k}_d \mathbf{H}^T \mathbf{Z} &= \widehat{\varphi} \ddot{\mathbf{x}}_g + \Gamma \mathbf{u} \\ \mathbf{M} &= \begin{bmatrix} \widehat{\mathbf{M}}_s & \mathbf{0} \\ \mathbf{0} & \mathbf{m}_d \end{bmatrix}; \mathbf{C} = \begin{bmatrix} \widehat{\mathbf{C}}_s & \mathbf{0} \\ \mathbf{0} & \mathbf{0} \end{bmatrix}; \mathbf{K} = \begin{bmatrix} \widehat{\mathbf{K}}_s & \mathbf{0} \\ \mathbf{0} & \mathbf{0} \end{bmatrix}; \\ \mathbf{H} &= \begin{bmatrix} -\Phi^T \mathbf{P}_g^T \\ \mathbf{I} \end{bmatrix}; \widehat{\varphi} = \begin{bmatrix} -\Phi^T \mathbf{M}_s \delta \\ -\mathbf{m}_d \mathbf{I} \end{bmatrix}; \Gamma = \begin{bmatrix} -\Phi^T \mathbf{P}_g^T \delta_d \\ \delta_d \end{bmatrix} \end{aligned} \quad (8)$$

where δ_d is the transformation matrix of the dampers' outputs.

Defining the state vector $\mathbf{X}=[\mathbf{Z}; \dot{\mathbf{Z}}]$, the state space equation can be denoted as

$$\begin{cases} \dot{\mathbf{X}}(t) = \mathbf{A} \mathbf{X}(t) + \mathbf{B} \mathbf{u}(t) + \mathbf{E} \mathbf{w}(t) \\ \mathbf{p}(t) = \mathbf{C} \mathbf{X}(t) + \mathbf{D} \mathbf{u}(t) \end{cases} \quad (9)$$

$$\mathbf{A} = \begin{bmatrix} \mathbf{0} & \mathbf{I}_p \\ -\mathbf{M}^{-1} \mathbf{K}^* & -\mathbf{M}^{-1} \mathbf{C}^* \end{bmatrix}; \mathbf{B} = \begin{bmatrix} \mathbf{0} & \mathbf{M}^{-1} \Gamma \end{bmatrix}$$

$$\mathbf{E} = \begin{bmatrix} \mathbf{0} & \mathbf{M}^{-1} \widehat{\varphi} \end{bmatrix}; \mathbf{K}^* = \mathbf{K} + \mathbf{H} \mathbf{k}_d \mathbf{H}^T; \mathbf{C}^* = \mathbf{C} + \mathbf{H} \mathbf{c}_d \mathbf{H}^T$$

where \mathbf{u} is the control force of the damper; \mathbf{w} is the excitation to the system.

3.3 Intermittent function in different state

According to the design of state switching of H-TMD, the whole state space is divided into such partitions $\mathbf{R}_1, \mathbf{R}_2, \mathbf{R}_3, \dots, \mathbf{R}_n$. The boundary conditions of such partitions \mathbf{R}_i are defined as the constraint equations of state variable $\mathbf{x}_i(t)$, control variable $\mathbf{u}_i(t)$ and disturbance input variable \mathbf{w}_i , that is $\mathbf{R}_i = \{f(\mathbf{x}_i, \mathbf{u}_i, \mathbf{w}_i) < \mathbf{c}\}$.

Considering the state-switching design of H-TMD, the condition of state partition is described as $\mathbf{R}_i = \{\Delta_{\min} \leq \mathbf{V} \mathbf{x} \leq \Delta_{\max}\}$, where \mathbf{V} as a transfer matrix of monitoring displacement and $\Delta_{\min}, \Delta_{\max}$ are upper and lower threshold vectors of monitoring displacement. All of the partitions which are independent with each other consist of the whole state space, and they are satisfied with

$$\bigcup_{i=1}^n \mathbf{R}_i = \mathbf{I}, \quad \bigcap_{i,j=1, \dots, n, i \neq j} \mathbf{R}_i \mathbf{R}_j = \mathbf{O}.$$

$$\dot{\mathbf{X}}(t) =$$

$$\begin{cases} \mathbf{A}_1 \mathbf{x}(t) + \mathbf{B}_1 \mathbf{u}(t) + \mathbf{E}_1 \mathbf{w}(t) & \mathbf{x}_1(t), \mathbf{u}_1(t), \mathbf{w}_1(t) \in \mathbf{R}_1 \\ \mathbf{A}_2 \mathbf{x}(t) + \mathbf{B}_2 \mathbf{u}(t) + \mathbf{E}_2 \mathbf{w}(t) & \mathbf{x}_2(t), \mathbf{u}_2(t), \mathbf{w}_2(t) \in \mathbf{R}_2 \\ \dots \\ \mathbf{A}_i \mathbf{x}(t) + \mathbf{B}_i \mathbf{u}(t) + \mathbf{E}_i \mathbf{w}(t) & \mathbf{x}_i(t), \mathbf{u}_i(t), \mathbf{w}_i(t) \in \mathbf{R}_i \end{cases} \quad (10)$$

Each H-TMD which is installed in the structure has two independent control states, so 2^m partitions need to be divided in a m numbers of H-TMDs included system. The state space models of very partitions are re-built according

to the different control state respectively, and the partition model of the system is expressed as Eq. (10).

The control gain of every partition is designed respectively according to the specific partition equation to realize the optimum control of the whole state space.

3.4 Introduction of logical variables

Logical variables are introduced with regard to the constrains of the segmented state space equations as shown in Eq. (11).

$$\mathbf{R}_i = \{\Delta_{\min} \leq \mathbf{V} \mathbf{x} \leq \Delta_{\max}\} \Leftrightarrow \begin{cases} \delta_1 \Leftrightarrow \mathbf{V} \mathbf{x} \geq \Delta_{\min} \\ \delta_2 \Leftrightarrow \mathbf{V} \mathbf{x} < \Delta_{\max} \\ \delta = \delta_1 \delta_2 \end{cases} \quad (11)$$

Two inequalities can be generated and shown as Eq. (4) along with a logical variable is introduced. Then the simple proposition δ_i is transformed into compound proposition, such as $\delta = \delta_1 \delta_2$, and the mixed integer linear inequalities can be inferred by Eq. (5).

3.5 Introduction of auxiliary variables

The instrumental variables are introduced as the product of the logical variable and continuous variable to express their coupling relationship. Assuming that logical variable δ is equal to constrains $\mathbf{R}_i = \{\Delta_{\min} \leq \mathbf{V} \mathbf{x} \leq \Delta_{\max}\}$ of segmented state equation $\mathbf{g}_i(\mathbf{x}, \mathbf{u}, \mathbf{w})$ and the auxiliary variable \mathbf{Z} is defined as the product of them, $\mathbf{Z} = \delta \mathbf{g}_i(\mathbf{x}, \mathbf{u}, \mathbf{w})$. According to the bound of the equation $\mathbf{g}_i(\mathbf{x}, \mathbf{u}, \mathbf{w})$, four inequalities can be inferred by Eq. (5) along with auxiliary variables are introduced.

3.6 The standardization model of MLD

The segmented state space equations can be integrated as an overall model consisted of evolution equation and output equation which included logical and auxiliary variables. The inequalities are inferred because of the introduction of logical and auxiliary variables are the constraint conditions of the whole hybrid model. The hybrid model can be inferred to be standardization model as shown in Eq. (1).

4. Simulation and analysis

4.1 Structure model and dynamic analysis

The 3rd Nanjing Yangtze River Bridge is selected as an example to demonstrate the proposed model. The bridge was designed with span arrangement as (63 m+257 m+648 m +257 m+63 m) and tower height of 215 m. Each tower has four cross girders which connect its two pylons. The lower parts of the pylons and the lowest cross girder are made by reinforced concrete and the other parts of the tower are made of steel.

Fig. 3 shows the Finite Element (FE) model of the bridge. In this model, the herringbone model is employed to reduce the amount of degrees of freedoms. The girder and

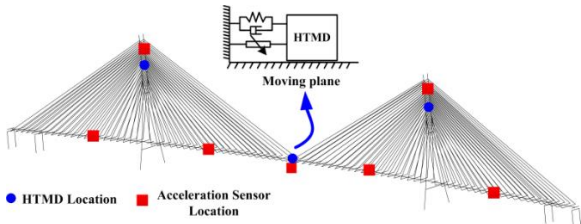


Fig. 3 FE model and devices' locations

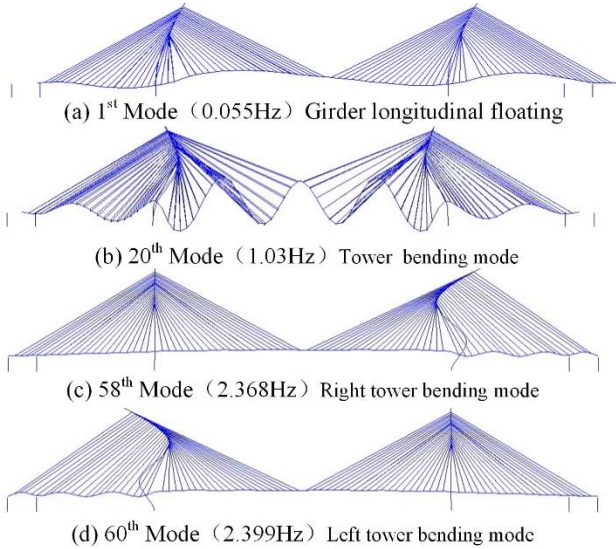


Fig. 4 Major mode shapes in longitudinal direction

Table 1 Modal frequencies and mode shapes of the model

Modes	Natural frequency (Hz)	Mode shape
1	0.055	Tower bending girder longitudinal floating
20	1.030	Tower bending
26	1.192	Tower bending
32	1.355	Tower bending
47	1.982	girder longitudinal floating
58	2.368	Right tower bending
60	2.399	Left tower bending

the tower are simulated by spatial beam elements. The cable is simulated by spatial link element and the influence of the cable sag effect is considered by Earnst equivalent elastic modulus. The rigid arms with large stiffness are built by spatial beam elements to connect the cable and the girder. For simplicity analysis, the interaction of pile and soil is ignored.

The FE modal analyses are conducted, the natural modal frequencies and the major mode shapes in longitudinal direction are shown in Table 1 and Fig. 4.

The structural parameters such as mass and stiffness matrix can be extracted from FE model. With the suggestion of Chinese specification (JTG/TB02-01 2008), the modal damping ratios of first and second modes are valued as 0.005, and the damping matrix is obtained by Rayleigh damping method. The transfer function curve of the structural key sections' responses can be achieved to analyze the main contributed modes. As examples, the

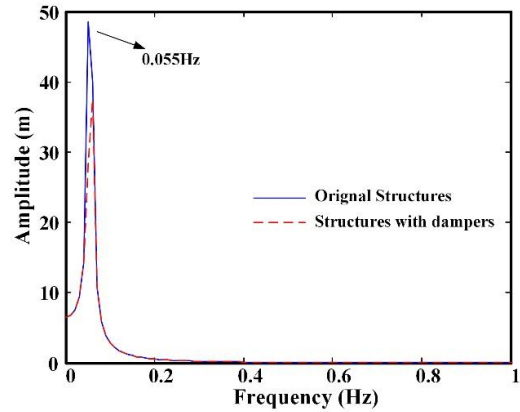


Fig. 5 Transfer function curve of displacement in mid-span

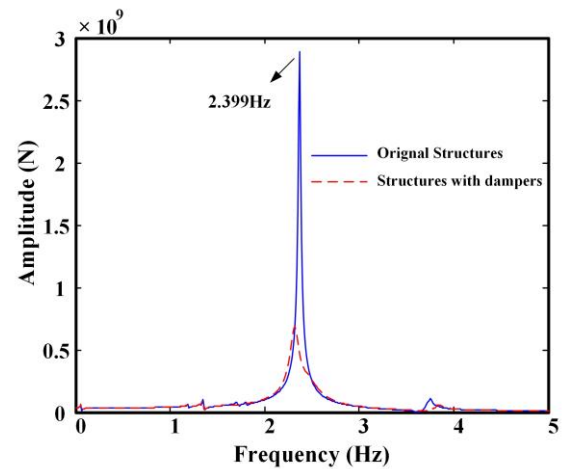


Fig. 6 Transfer function curve of shear force in right tower bottom

transfer function curve of the displacement in mid-span and shear force in the right tower bottom are shown in Fig. 5 and Fig. 6.

The dynamic analysis results point out that the primary modes are girder longitudinal floating mode and tower bending modes. The longitudinal excitation correspond to the larger response of the mid-span displacement and shear and moment of the tower bottom. The primary mode of mid-span displacement is first mode and the primary modes of towers are 58th and 60th modes.

4.2 Control design

The control scheme is designed for three targeted modes including 1st mode, 58th mode and 60th mode. As shown in Fig. 3, a H-TMD is installed at the mid-span to tune the first mode and two H-TMDs are placed at the upper cross girders of two towers for tuning 58th mode and 60th mode. By choosing the mass ratio of 1%, the damper mass is 350 ton for the first damper and is 50 ton for the second and third dampers. The stiffness and damping parameters of H-TMD are similar to TMD. In this study, the damper parameters are determined by the H₂ gradient optimization method (Wen *et al.* 2017) which is a global optimization method to solve distributed vibration dampers and multi-

Table 2 Locations and parameter values of H-TMD devices

No.	Installation Location	Mass (ton)	Frequency ratio f_{opt}	Damping ratio γ_{opt}
1	Mid-span	350	0.984	0.05
2	Upper cross girder of left tower	50	0.951	0.088
3	Upper cross girder of right tower	50	0.951	0.088

object problems. In the process of parameter optimization, output vector is given as $\mathbf{z}=[\mathbf{u}_m \mathbf{V}_l \mathbf{M}_l \mathbf{V}_r \mathbf{M}_r]^T$, where \mathbf{u}_m , \mathbf{V}_l , \mathbf{M}_l , \mathbf{V}_r and \mathbf{M}_r are mid-span displacement, shear and moment of the left tower bottom and the right tower bottom respectively. The weight of output vector is chosen as $\boldsymbol{\lambda}=\text{diag}([30 \ 7 \times 10^{-7} \ 1.5 \times 10^{-8} \ 10^{-7} \ 3.5 \times 10^{-9}])$, and the optimal parameters of the dampers are shown in Table 2. The transfer function curves of bridges-dampers system with the adopted parameter values are shown in Fig. 5 and Fig. 6. The comparisons with the ones of original structure show that the dampers significantly reduce the amplitude of transfer function near the tuned modes, and the designed parameters of dampers are effective.

The optimal control in the stage of passive control can be achieved by the parameter optimization of H-TMDs. In the stage of active control, the optimal control should be realized by the design of the control algorithm. In this case, H_2 control algorithm is used and the design output vector is also expressed as $\mathbf{z}=[\mathbf{u}_m \mathbf{V}_l \mathbf{M}_l \mathbf{V}_r \mathbf{M}_r]^T$. The output weight is designed as $\mathbf{Q}=\text{diag}([10^{-3} \ 3 \times 10^{-4} \ 3 \times 10^{-4} \ 10^{-5} \ 10^{-5}])$ and the input weight is given as $\mathbf{R}=\mathbf{I}_{5 \times 5}$. After that, the control force can be determined by $\mathbf{u}=-\mathbf{G}\mathbf{x}$, where \mathbf{G} is control gain and \mathbf{x} is the state vector of the whole model. The sensor layout design and Kalman-Bucy filter are selected to estimate the whole model for that it is not possibly measure the whole structural state directly. The acceleration sensors are installed as shown in Fig. 3 and their directions are all longitudinal.

The H-TMD state switching design is in conformity with that proposed in Section 3 and the displacement switch thresholds of the dampers are set as 0.2 m.

Based on the control design and the fundamental theory of MLD model, the bridge-MLD model system can be yielded by Eqs. (4)-(10). The standardization model is shown as Eq. (1).

4.3 Results and analysis

In order to verify the performance of the HTMD systems, 40 earthquake ground motions are selected from PEER Ground Motion Database based on the target acceleration spectrum which is determined by the site condition and the specification of Chinese code (JTG/TB02-01 2008). These records with different frequency components and with dominant frequencies covering the fundamental natural frequency of the structure were considered for excitations. The basic information of the selected excitations are listed in Table 3. The spectral acceleration curves of target and selected ground motions is shown in Fig. 7.

The MLD model of bridge-HTMD system is built and simulated with the selected longitudinal excitation. The

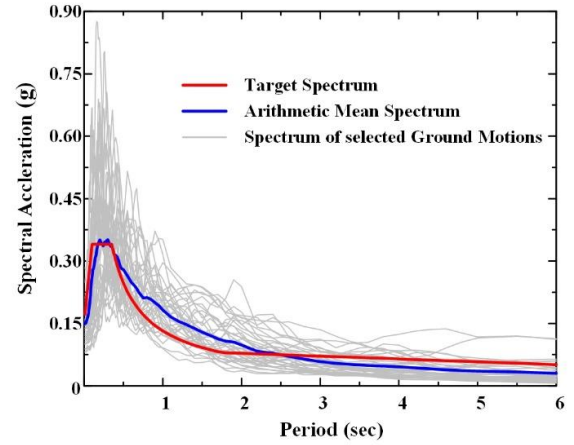


Fig. 7 Spectral acceleration curves of target and selected ground motions

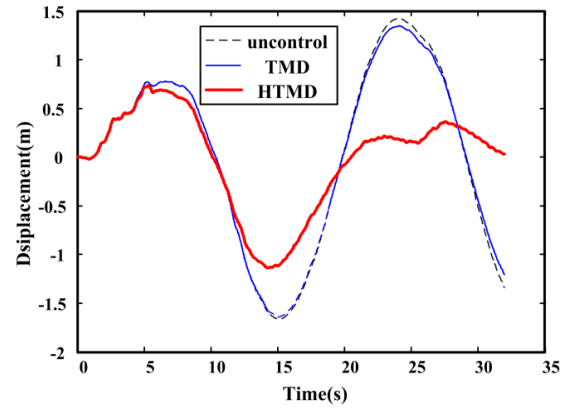


Fig. 8 Time-history curves of mid-span displacement

passive TMD control scheme, which has the same parameters and locations with proposed H-TMD design, is simulated at the same time to make comparisons. The case under excitation of El Centro north-south (NS) component of the 1940 Imperial Valley Earthquake (No.1 in Table 3) is taken as an example to show the structural responses with or without dampers. Fig.8 shows the time-history curves of the mid-span displacement. The time-history curves of the bending moment in left tower bottom and shear force in right tower bottom are shown in Fig. 9 and Fig. 10, respectively.

In order to make a better quantitative comparisons of control effect, 10 indices are defined and analyzed. In which, J1-J5 are the peak indices of mid-span displacement, shear and moment in left tower bottom, and shear and moment in right tower bottom respectively; and J6-J10 are their RMS indices. The peak index is defined as Eq. (12) and the RMS index is expressed as Eq. (13), in which $a_{ctr}(t)$, $a_{unctr}(t)$ are the structural target time-histories responses with different control schemes and uncontrolled states, t_s is end the time of excitations, $a_{ctr}^{\max} = \max(a_{ctr}(t))$, and $a_{unctr}^{\max} = \max(a_{unctr}(t))$.

$$J_{peak} = a_{ctr}^{\max} / a_{unctr}^{\max} \quad (12)$$

Table 3 Basic information of selected earthquake ground motions

No.	Year	Station Name	No.	Year	Station Name	No.	Year	Station Name
1	1940	"El Centro Array #9"	15	1966	Cholame-Shandon Array #8	29	1971	Maricopa Array #3
2	1995	Kobe University	16	1968	El Centro Array #9	30	1971	Pacoima Dam (upper left abut)
3	1971	San Fernando-Whittier Narrows Dam	17	1968	LA-Hollywood Stor FF	31	1971	Pasadena-CIT Athenaeum
4	1942	El Centro Array #9	18	1968	LB-Terminal Island	32	1971	Port Hueneme
5	1952	LA - Hollywood Stor FF	19	1968	Pasadena-CIT Athenaeum	33	1971	Puddingstone Dam (Abutment)
6	1952	Pasadena - CIT Athenaeum	20	1968	San Onofre-So Cal Edison	34	1971	San Juan Capistrano
7	1952	Santa Barbara Courthouse	21	1971	Buena Vista-Taft	35	1971	San Onofre-So Cal Edison
8	1952	Taft Lincoln School	22	1971	2516 Via Tejon PV	36	1971	Santa Felita Dam (Outlet)
9	1952	San Luis Obispo	23	1971	Carbon Canyon Dam"	37	1971	UCSB - Fluid Mech Lab
10	1953	El Centro Array #9	24	1971	Cedar Springs_ Allen Ranch	38	1971	Wheeler Ridge - Ground
11	1954	Ferndale City Hall	25	1971	LA - Hollywood Stor FF	39	1971	Wrightwood-6074 Park Dr
12	1956	El Centro Array #9	26	1971	LB - Terminal Island	40	1972	Managua_ ESSO
13	1961	Hollister City Hall	27	1971	Maricopa Array #1			
14	1966	Cholame-Shandon Array #12	28	1971	Maricopa Array #2			

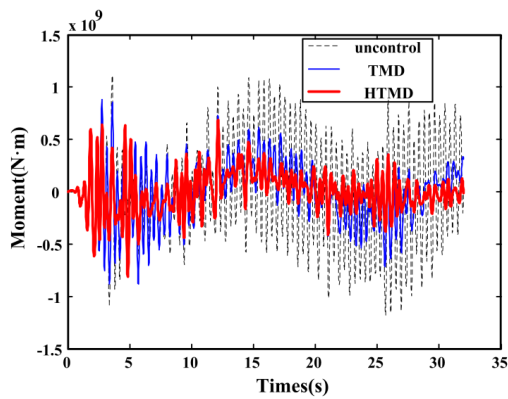


Fig. 9 Time-history curves of moment in left tower bottom

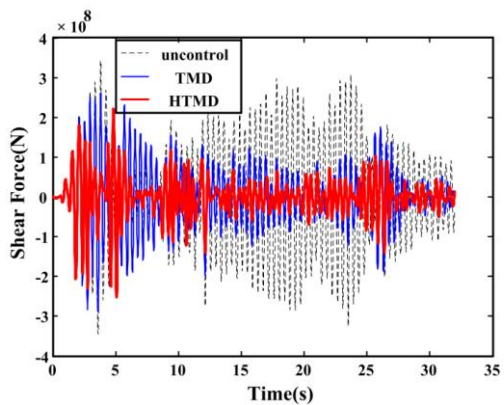


Fig. 10 Time-history curves of shear force in right tower bottom

$$J_{RMS} = \frac{\sum_{t=0}^{t=t_s} a_{ctr}^2(t)}{\sum_{t=0}^{t=t_s} a_{unctr}^2(t)} \quad (13)$$

Fig. 11 shows the values of J2 indices under excitation of 40 different ground motions. It is obvious that both two control schemes contribute to the control effect and the H-TMD system reveal a better results in most cases. Because TMD only contribute to the limited tuned modes and the

Table 4 Control effects comparisons between two control schemes

Evaluation Indices	Control Schemes	
	TMD	H-TMD
J1	0.9729	0.9054
J2	0.7326	0.6574
J3	0.7313	0.6515
J4	0.7194	0.6315
J5	0.7249	0.6276
J6	0.9238	0.7985
J7	0.3120	0.2389
J8	0.3642	0.2514
J9	0.2668	0.1970
J10	0.2691	0.1828

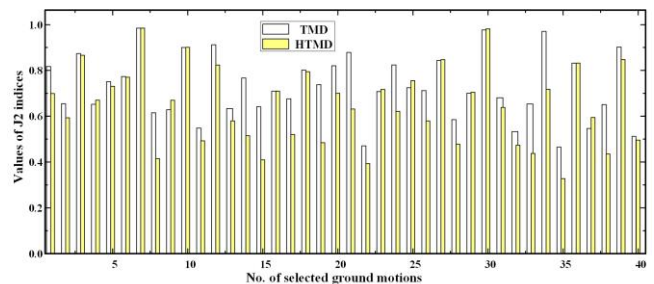


Fig. 11 Values of J2 indices under different ground motions excitation

effects are restricted. While H-TMD-hybrid control method can play better effects to reduce the peak and RMS indices by applying control force to the structure except the tuning effect when the structural responses are beyond the threshold. For brevity, the other indices are not listed one by one, but the average values of evaluation indices under 40 excitations are listed in Table 4.

4.4 Discussion

The selective control according to the structural

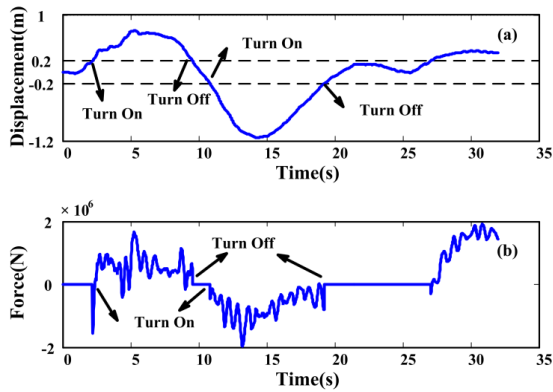


Fig. 12 Schematic of H-TMD state-switching: (a) displacement(m); (b) control force(N)

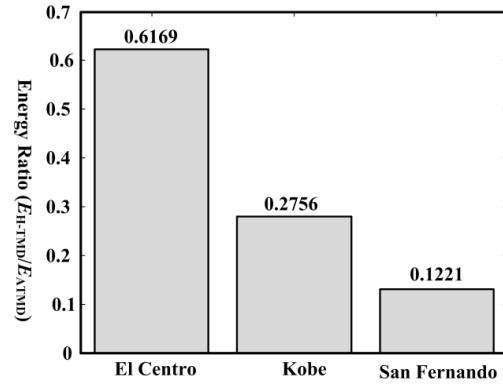


Fig. 13 Energy consumption ratio of H-TMD to ATMD under three wave excitations

monitoring response is the main characteristic of the proposed hybrid control method. It means that the consumed energy mainly contribute to reduce the excessive response beyond the threshold, which leads to less energy consumption than traditional active control methods.

The schematic of H-TMD state-switching is shown in Fig. 12. The relationship between the mid-span monitoring displacement and time is shown in Fig. 12(a). Fig. 12(b) shows the relationship between the control force of the H-TMD, which is installed on the mid-span, and time. In the initial stage of excitation, the structural response is less than the threshold (0.2 m) so that the damper plays by the role of passive TMD without control force. When the monitoring displacement response reaches the switch threshold, the damper switches to active control state and acts active control force to the bridge for vibration reduction. The schematic shows that the proposed hybrid model can realize the state-switching according to the structural real-time response to mitigate the structure vibrations.

During the vibration of the bridge, both H-TMD and ATMD dampers provide control force to bridge by

consuming energy. The total energy consumption can be expressed as

$$E = \sum_{i=1}^n \int_0^{t_s} f_{di}(t) s_i(t) dt \quad (14)$$

where n is the number of attached active dampers, $f_{di}(t)$ is control force of the i^{th} damper, and $s_i(t)$ is the structure response where i^{th} damper is installed.

To analyze the energy consumption of H-TMD system, cases under three excitations are selected including El Centro 1940 earthquake, Kobe 1995 earthquake and San Fernando 1971 earthquake (the first three ground motions in Table 3) to analyze the energy consumption of the bridge-HTMDs system and the bridge-ATMDs system. In the bridge-ATMDs system, ATMD dampers are chosen with the same installed locations, parameters and control gain design of the H-TMDs as in the above analysis. Unlike H-TMDs, ATMD dampers provide control force in the whole process without switching. The energy consumption ratio of H-TMD to ATMD schemes under three wave excitations are

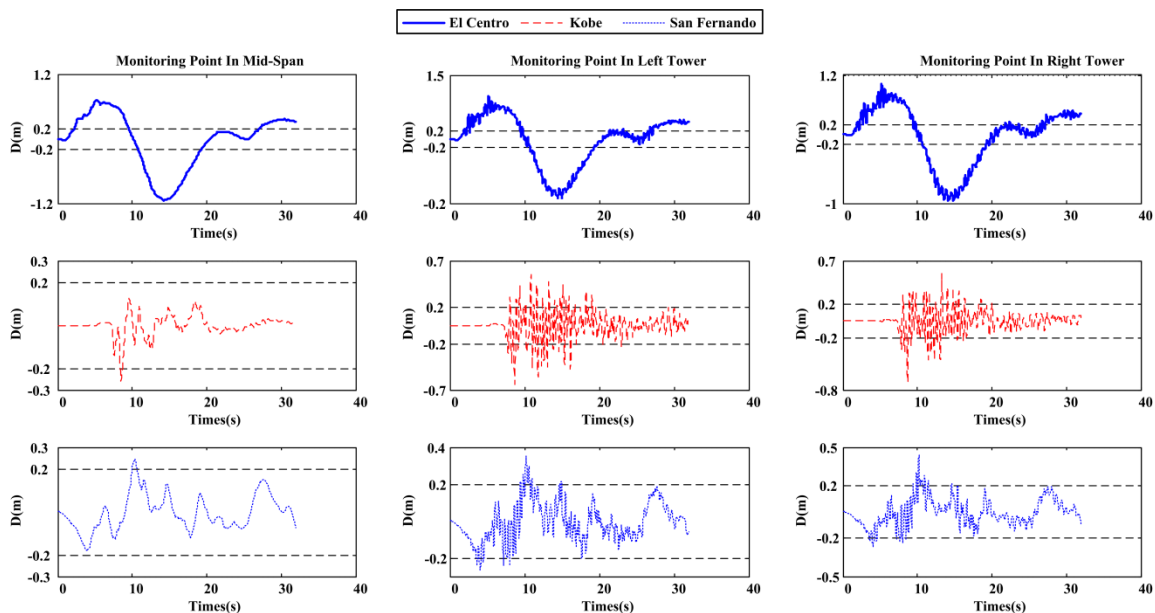


Fig. 14 Monitoring responses under three wave excitations

shown in Fig. 13 and the monitoring responses of bridge are shown in Fig. 14.

The results indicate less energy consumption of H-TMD scheme compared with that of ATMD scheme for all three wave excitations. Under San Fernando earthquake excitation, the energy consumption ratio of H-TMD to ATMD schemes reaches to the minimum value of three cases, for that all monitoring responses are less than the designed threshold (0.2 m). The passive control state plays a major role in the whole process, and it is adequate for small vibration within threshold. However, under El Centro earthquake excitation, there are more structure responses which are beyond the thresholds, so that major energy is consumed to provide active force for mitigation of the oversized vibrations. In this way, the proposed method demonstrates that its advantages are the energy conservation and intelligent decision.

5. Conclusions

Based on H-TMD and MLD model, this paper proposed a new hybrid method to control the vibrations of the long span cable stayed bridge. The establishing process and the design method of the hybrid control model were described in detail. Further, a case study was presented and carried out to verify the control effects of the proposed model. The following conclusions were drawn:

- The proposed H-TMD-hybrid control model can switch between different control states as the designed state-switching conditions. The results of the case study reveal that this method performed a better performance on the control effects than passive control method. More importantly, it is good at control state decision of dampers according to the relationship of structural response and designed threshold, and its energy consumption is less than that of ATMD.
- This paper is an exploratory research and a novel research idea for the application of the hybrid system in the field of the structure vibration control. However, experimental studies are necessary to reinforce the present theoretical work and optimization control design of the hybrid system is also essentially carried out by further studies in the future.

Acknowledgments

The research described in this paper was financially supported by Special Scientific Research Fund of Transport Ministry in China (Grant Nos. 2011318223170), China National Natural Science Foundation (Grant Nos. 51678030) and the Transportation Science and Technology Program of Hebei Province (Grant No. QG2018-8). All members of the project team is gratefully acknowledged for their supports to our work.

References

Askari, M., Li, J. and Samali, B. (2016), "Semi-active control of

- smart building-MR damper systems using novel TSK-Inv and max-min algorithms", *Smart. Struct. Syst.*, **18**(5), 1005-1028.
- Bemporad, A. and Morari, M. (1999), "Control of systems integrating logic, dynamics, and constraints", *Automatica*, **35**(3), 407-427.
- Ghorbani-Tanha, A.K., Rahimian, M. and Noorzad, A. (2011), "A novel semiactive variable stiffness device and its application in a new semiactive tuned vibration absorber", *J. Eng. Mech.*, **137**(6), 390-399.
- Guezar, F.E., Bouzahir, H. and Fournier-Prunaret, D. (2011), "Event detection occurrence for planar piece-wise affine hybrid systems", *Nonlin. Anal. Hybrid Syst.*, **5**(4), 626-638.
- He, Y.C. and Li, Q. (2014), "Dynamic responses of a 492-m-high tall building with active tuned mass damping system during a typhoon", *Struct. Control. Hlth. Monit.*, **21**(5), 705-720.
- Huang, X. (2018), "Evaluation of genetic algorithms for the optimum distribution of viscous dampers in steel frames under strong earthquakes", *Earthq. Struct.*, **14**(3), 215-227.
- Ikago, K., Saito, K. and Inoue, N. (2012), "Seismic control of single-degree-of-freedom structure using tuned viscous mass damper", *Earthq. Eng. Struct. Dyn.*, **41**(3), 453-474.
- Lin, P.Y., Lin, T.K. and Hwang, J.S. (2013), "A semi-active mass damping system for low- and mid-rise buildings", *Earthq. Struct.*, **4**(1), 63-84.
- Ministry of Transport of the People's Republic of China (2008), *Seismic Resistance Design Specification of Highway Bridges (JTG/T TB02-01)*, China Communications Press, Beijing, China.
- Nigdeli, S.M. and Boduroğlu, M.H. (2013), "Active tendon control of torsionally irregular structures under near-fault ground motion excitation", *Comput. Aid. Civil Infrastr. Eng.*, **28**(9), 718-736.
- Nimmen, K.V., Verbeke, P., Lombaert, G., Roeck, G.D. and Broeck, P.V.D. (2016), "Numerical and experimental evaluation of the dynamic performance of a footbridge with tuned mass dampers", *J. Bridge Eng.*, **21**(8), C4016001.
- Pourzeynali, S., Salimi, S., Yousefifefat, M. and Kalesar, H.E. (2016), "Robust multi-objective optimization of STMD device to mitigate buildings vibrations", *Earthq. Struct.*, **11**(2), 347-369.
- Quaranta, G., Mollaioli, F. and Monti, G. (2016), "Effectiveness of design procedures for linear TMD installed on inelastic structures under pulse-like ground motion", *Earthq. Struct.*, **10**(1), 239-260.
- Sirmatel, I.I. and Geroliminis, N. (2018), "Mixed logical dynamical modeling and hybrid model predictive control of public transport operations", *Tran. Res. Pt. B-Meth.*, **114**, 325-345.
- Sun, X., Cai, Y., Wang, S., Xu, X. and Chen, L. (2019), "Optimal control of intelligent vehicle longitudinal dynamics via hybrid model predictive control", *Robot. Auton. Syst.*, **112**, 190-200.
- Sun, X., Yuan, C., Cai, Y., Wang, S. and Chen, L. (2017), "Model predictive control of an air suspension system with damping multi-mode switching damper based on hybrid model", *Mech. Syst. Signal Pr.*, **94**, 94-110.
- Venanzi, I., Ubertini, F. and Materazzi, A.L. (2013), "Optimal design of an array of active tuned mass dampers for wind-exposed high-rise buildings", *Struct. Control. Hlth. Monit.*, **20**(6), 903-917.
- Vieira, A., Brogliato, B. and Prieur, C. (2017), "Preliminary results on the optimal control of linear complementarity systems", *IFAC-PapersOnLine*, **50**(1), 2977-2982.
- Wen, Y., Chen, Z. and Hua, X. (2017), "Design and evaluation of tuned inerter-based dampers for the seismic control of MDOF structures", *J. Struct. Eng.*, **143**(4), 04016207.
- Xing, C., Wang, H., Li, A. and Xu, Y. (2014), "Study on wind-induced vibration control of a long-span cable-stayed bridge

- using TMD-type counterweight”, *J. Bridge Eng.*, **19**(1), 141-148.
- Xu, Z., Agrawal, A.K. and Yang, J.N. (2006), “Semi-active and passive control of the phase I linear base-isolated benchmark building model”, *Struct. Control. Hlth. Monit.*, **13**(2-3), 626-648.
- Yan, W., Xu, W., Wang, J. and Chen, Y. (2014), “Experimental research on the effects of a tuned particle damper on a viaduct system under seismic loads”, *J. Bridge Eng.*, **19**(3), 04013004.
- Yu, C., Xiang, H., Li, Y. and Pan, M. (2018), “Optimization of longitudinal viscous dampers for a freight railway cable-stayed bridge under braking forces”, *Smart. Struct. Syst.*, **21**(5), 669-675.
- Yu, Z., Su, K. and Lin, J. (2009), “A smoothing Levenberg–Marquardt method for the extended linear complementarity problem”, *Appl. Math. Model.*, **33**(8), 3409-3420.

CC